NÖHÜ Müh. Bilim. Derg. / NOHU J. Eng. Sci., 2025; 14(1), 122-131

Niğde Ömer Halisdemir Üniversitesi Mühendislik Bilimleri Dergisi
Niğde Ömer Halisdemir University Journal of Engineering Sciences

Araştırma makalesi / Research article

www.dergipark.org.tr/tr/pub/ngumuh / www.dergipark.org.tr/en/pub/ngumuh

Spatial assessment of urban heat island (UHI) in Kütahya using Landsat-8 satellite data

Landsat-8 uydu verilerini kullanarak Kütahya'daki kentsel ısı adasının (UHI) mekansal değerlendirmesi

Ali Samet Öngen[1,*], Enes Zengin[2]

[1] *Kütahya Dumlupınar University, Faculty of Engineering, Department of Geological Engineering, 43100, Kütahya, Türkiye*
[2] *Kütahya Dumlupınar University, Faculty of Architecture, Department of Urban and Regional Planning, 43100, Kütahya, Türkiye*

Abstract

The Urban Heat Island (UHI) effect refers to the phenomenon where urban areas experience significantly higher temperatures than their rural surroundings due to human activities and modifications, such as replacing natural land cover with impervious surfaces, reducing vegetation, and increasing heat-absorbing materials. Kütahya central district has a dense population and building layout, which contributes to the intense UHI. Geographic Information System (GIS) and its tools are widely used in assessing UHI in urban areas, providing insights for both researchers and local authorities. The study aims to spatially evaluate the urban heat island in Kütahya using Landsat-8 satellite data. Landsat-8 images, operating in the 10.60 - 11.19 µm range acquired on August 8, 2023 (Path: 179, Row: 33, Cloud Cover: 0%) were utilized to create the Urban Heat Island (UHI) map for the study area. Through spatial analysis using Landsat-8 data for Kütahya city center, six different classes were defined, with the UHI map created using land surface temperature values. The highest and lowest UHI values vary between 4.245°C and -3.457°C. It has been observed that the average UHI increases by 12% in areas lacking dense building structures, characterized by rock surfaces and limited green areas. Conversely, in areas with parks, forests, and sparse settlements, the UHI decreases by 10%. With this study, a comprehensive evaluation of UHI was conducted for Kütahya city center. While the results obtained are expected to be an important resource for researchers and local authorities, they are also anticipated to be beneficial in the fields of engineering geology, urban geology, and urban planning.

Keywords: Kütahya, Landsat-8, Land surface temperature, Spatial analysis, Urban heat island

Öz

Kentsel Isı Adası (UHI) etkisi, şehir alanlarının, insan faaliyetleri ve değişiklikleri nedeniyle, kırsal çevreye göre önemli ölçüde daha yüksek sıcaklıklara maruz kalması olarak tanımlanabilir. Bu değişiklikler arasında doğal arazi örtüsünün geçirimsiz yüzeylerle değişmesi, bitki örtüsünün azalması ve ısıyı emen malzemelerin artması yer almaktadır. Kütahya merkez ilçesinin, yoğun nüfusu ve bina yerleşimi UHI etkisinin artmasına neden olmaktadır. Coğrafi Bilgi Sistemi (CBS) ve araçları, kentsel alanlardaki UHI'yi değerlendirmede yaygın olarak kullanılmakta olup, hem araştırmacılara hem de yerel yetkililere önemli bilgiler sunmaktadır. Çalışma kapsamında Landsat-8 uydu verileri kullanılarak Kütahya'daki kentsel ısı adasının mekansal olarak değerlendirilmesi amaçlanmıştır. Çalışma alanı için Kentsel Isı Adası (UHI) haritası oluşturmak amacıyla 8 Ağustos 2023'te (Path: 179, Row: 33, Cloud Cover: %0) alınan Landsat-8 görüntüleri kullanılmış, 10.60 - 11.19 µm aralığında çalışan verilerinden yararlanılmıştır. Kütahya şehir merkezi için Landsat-8 verileri kullanılarak yapılan mekansal analizle altı farklı sınıf tanımlanmış olup, arazi yüzey sıcaklığı değerleri kullanılarak UHI haritası oluşturulmuştur. En yüksek ve en düşük UHI değerleri sırasıyla 4.245°C ile -3.457°C arasında değişmektedir. Yoğun bina yapısının bulunmadığı, kaya yüzeyleri ve sınırlı yeşil alanlarla karakterize edilen bölgelerde ortalama UHI'nin %12 arttığı gözlemlenmiştir. Buna karşılık, parklar, ormanlar ve seyrek yerleşim alanları olan bölgelerde UHI %10 azalmaktadır. Bu çalışma ile Kütahya şehir merkezi için kapsamlı bir UHI değerlendirmesi yapılmıştır. Elde edilen sonuçların araştırmacılar ve yerel yetkililer için önemli bir kaynak olması beklenirken, mühendislik jeolojisi, kentsel jeoloji ve şehir planlama alanlarında da faydalı olması öngörülmektedir.

Anahtar Kelimeler: Kütahya, Landsat-8, Yüzey sıcaklığı, Mekansal analiz, Kentsel ısı adası

1 Introduction

Urban areas are experiencing increased crowding due to various economic, cultural, and social factors. The rising population in urban centers leads to an increase in rapid urbanization [1]. As a result, green spaces are being replaced by man-made artificial surfaces (buildings, pavements, asphalt, bridges, subway tunnels, etc.). Artificial surfaces in city centers absorb solar heat energy, leading to higher air temperatures compared to the surrounding rural areas. This phenomenon, initially explored by [2], is known as the Urban

* Sorumlu yazar / Corresponding author, e-posta / e-mail: alisamet.ongen@dpu.edu.tr (A. S. Öngen)
Geliş / Recieved: 02.08.2024 Kabul / Accepted: 23.10.2024 Yayımlanma / Published: 15.01.2025
doi: 10.28948/ngumuh.1527341

Heat Island (UHI) effect. Consequently, air temperatures in urban areas can be up to 10°C warmer than those in rural regions [3-5]. Alterations in land use and cover can impact ecosystems on multiple scales, ranging from local areas to the global landscape, and play a significant role in the progression of climate change. UHI, stands as a key contributor to these climate alterations [6]. One of the main reasons for UHI is the lack of vegetation in urban spaces and population-dense districts [7]. Plants release solar rays back into the atmosphere through evapotranspiration (evaporation and transpiration). With increased urbanization and the consequent reduction of green spaces, evapotranspiration decreases, and solar rays are trapped by artificial surfaces. This replacement of natural vegetation with artificial surfaces is a primary cause of the urban heat island effect, leading to higher air temperatures in city centers compared to rural areas. Temperature measured on an asphalt surface during the daytime can be 20°C higher than on grass. [8], It is also noted that cover materials like concrete and asphalt absorb 60-95% of incoming solar rays, reflecting only 5-40% back [9] . Human-made structures such as buildings, pavements, filled areas, subway tunnels, electrical cables, district heating systems, and sewage systems contribute to the urban heat island effect [10,11], Additionally, fluctuations in LST between day and night also influence the UHI effect. Numerous studies have emphasized the substantial temperature increase in urban centers compared to rural areas [9, 12-15]. This temperature rise is attributed not only to climatic factors but also to the UHI effect [16]. Research in Istanbul examined the link between population growth and the UHI effect, revealing that in the densely constructed southern part of Istanbul, the average air temperature has risen by 0.47°C over the past 40 years, while in the less developed northern part, it has decreased by 1.17°C [17]. This suggests that temperature increases in urban centers result from both climatic factors and the UHI effect. Similarly, [18]) in Istanbul highlighted that the UHI factor correlates with population and city size. However, the UHI effect is not limited to large cities; it is also observed in small and medium-sized cities [19]. A similar study carried out by [20] with a different perspective to focus on UHI and geothermal energy potential in Kütahya. This effect depends on various factors such as topography, the density of human-made structures, weather conditions, and the presence and distribution of parks and gardens within the city. Urban areas with more green spaces can alleviate the UHI effect. It is also noted that the UHI effect exhibits heterogeneous distribution within a city and is a locally specific concept. Consequently, the intensity of the UHI shows variations within a city depending on the types of areas in the city center, such as buildings, structures, parks, green zones, etc. Geographic Information Systems (GIS) and its tools are widely used by researchers in earth science, offering diverse perspectives on various focus areas such as geological mapping, climate change, natural resource management, disaster response, earthquakes, image processing, micro and macro feature extraction, environmental monitoring, and urban planning and geology [21-30]. Mapping analysis as a part of GIS can be used to explore, illustrate and analyze the UHI phenomenon. In order to assess the UHI effect with Landsat-8 imagery, scientists use the thermal infrared data from the Thermal Infrared Sensor (TIRS). This process includes selecting Landsat-8 images of the study area with the least cloud cover and from comparable seasons for accurate comparison in terms of time series. These images can then be analyzed to process the raw satellite data into land surface temperature datasets using GIS-based programs like ArcGIS, QGIS, etc. It is also possible to detect warmer urban areas by correlating the temperature dataset with land cover information from satellite data. This also helps to measure the UHI effect and its severity within urban districts and neighboring rural regions to identify the parameters contributing to UHI. Landsat 8 data was used from 2014 to 2016 to analyze the surface UHI effects in Bangkok, to identify temperature distribution in dense urban areas, and to provide detailed information for mitigation strategies as a part of environmental sustainability, urban planning and policymakers [31]. Another methodology was developed using Landsat 8 thermal infrared images to detect and analyze UHI, providing data for urban planning and improving thermal comfort in cities by monitoring temperature anomalies over time [32]. As part of a study focusing on the surface UHI effect in Stuttgart (Germany) using Landsat-8 data show that a decrease in surface UHI by 1.4°C from 2004-2008 to 2016-2020, while there is a 2.5°C rise in land surface temperature, which shows land cover changes, is key factors affecting local temperature variations, important for urban planning and policy evaluation [33]. A study assessed the surface UHI effect in Bursa, Türkiye for a time frame from 2002 to 2020 by using Landsat 7-8 images to analyze changes in land use/land cover (LULC) and land surface temperature (LST), implementing indices like NDVI to classify urban, vegetation, and water zones, reveals an overall increase in LST and significant growth in SUHI intensity over the last 18 years [34]. Urban Heat Island (UHI) effects across different local climate zones in Bragança, Portugal, utilizing air temperature data, Landsat 8 imagery, and on-site measurements were also investigated [35]. A new method was developed, using Landsat imagery, to accurately map UHI in Nanjing, China, from 2000 to 2021, revealing a correlation between urban development, green space expansion, and changes in UHI intensity [36]. In Kütahya, located in the western part of Turkey, population and urbanization continuously increase (Figure 1). As the population grows, new areas are being developed, urbanization rates are rising, and the amount of agricultural and green spaces is diminishing. This trend increases the likelihood of the emergence or intensification of the urban heat island effect in city centers. This study aims to detect and analyze UHI in Kütahya using Landsat-8 satellite imagery from August 2023. The research intends to identify temperature differences between urban/rural areas and the spatial analysis of the UHI effect, thereby contributing to urban planning and environmental management strategies.

2 Methodology

2.1 Study area

Kütahya, located on the border of the Aegean and

Central Anatolia regions, lies between the northern latitudes of 38°70' and 39°80' and the eastern longitudes of 29°00' and 30°30'. With an area of 12.014 km², Kutahya comprises approximately 1.5% of Turkey's land according to the Turkish Statistical Institute (TÜIK, 2023). It is bordered by the provinces of Bursa, Bilecik, Eskişehir, Afyonkarahisar, Uşak, Manisa, and Balıkesir. The city center of Kütahya generally has a flat topography. The city is established on an alluvial plain irrigated by the Porsuk and Felent rivers, at the foothills of Yellice Mountain. The highest elevation in the city is Yellice Mountain, located south of the city, with a peak of 1901 meters. Due to the Kütahya Fault Zone, a sudden increase in slope is observed between the Kütahya Plain and Yellice Mountain. According to the TUIK Address-Based Population Registration System (ADNKS) statistics for 2023, the total population of Kütahya, including its districts, is 571.463. Approximately half of the total population (284.536 people) resides in the central district, which is more socially and economically developed compared to other districts. The urban population of the central district is 253.583, while the rural population is 30,953. TÜIK data shows that the rural population last increased between 1997 and 2000. Since then, there has been an increase in rural-to-urban migration, leading to a decrease in the rural population. Consequently, urbanization, which reduces green spaces, has continuously increased with the growing population. According to the ESRI Sentinel-2 Land Cover Explorer, in 2023, the land cover distribution for Kütahya is dominated by rangeland, which constitutes 36.39% of the total area. Cropland follows at 28.24%, and built-up areas cover 26.11%. Trees make up 8.65%, while bare ground represents 0.53%. Water bodies account for 0.07%, and flooded vegetation is minimal at 0.01%. Although Kütahya is in the Aegean region, it does not fully reflect the climate characteristics of the Aegean region due to its distance from the sea and its elevation. According to the [37] climate classification (1954), Kütahya falls under the CSB climate category (hot and dry summers, cool and wet winters). The temperature is influenced by Central Anatolia, while precipitation is affected by the Marmara region. The spring and autumn seasons are quite rainy. According to the State Meteorological Service (DMI), the highest monthly precipitation in Kütahya city center was observed in December, with 75.22 mm/month between 1970 and 2020. The annual average precipitation is 557.11 mm/year. During the same period, the annual average temperature is 10.81°C/year, with the lowest average temperature in January at 0.36°C/month and the highest average temperature in July at 21.00°C. In July, when temperatures are highest, precipitation drops to 18.37 mm/month.

2.2 Data collection

Landsat 8 imagery acquired from the USGS Earth Explorer for August 8th, 2023, Path: 179 Row: 33 with 0% cloud cover, was utilized for the assessment of UHI in Kütahya city center. The satellite imagery, belonging to Landsat Collection 2 Level 1, offers a comprehensive view of the cityscape at a moderate spatial resolution of 30 meters to provides to perform a generalized assessment, enabling the analysis of land surface temperatures and the identification of heat islands.

2.3 Land surface temperature (LST) retrieval from thermal band

Land surface temperature (LST) plays a pivotal role in the exchange of long-wave radiation and turbulent heat fluxes at the interface between the Earth's surface and the atmosphere. It is a key parameter that governs physical processes on surface energy and water balance from small to large scales from globally down to locally [38-40]. Measuring LST helps researchers understand the heat dynamics of different surfaces, monitor changes over time, and analyze UHI phenomena, which are areas of elevated temperatures within urban areas compared to their rural surroundings. LST data is typically obtained from satellite thermal infrared sensors, which capture the radiation emitted from the Earth's surface. These data help study climate change, land use patterns, ecosystem dynamics, and human-environment interactions and more. There are two thermal infrared sensors (TIRS) on Landsat 8; Band 10 and Band 11. These bands capture data in the long-wave infrared spectrum, with Band 10 operating between 10.60 - 11.19 µm and Band 11 between 11.50 - 12.51 µm. Each pixel in these bands represents a spatial resolution of 100 meters, which was resampled to 30 meters during Level-1 product generation, allowing for the estimation of LST with in more detail. The thermal data collected by Landsat 8 provides precise monitoring of temperature variations and the identification of thermal anomalies, which is important for applications such as UHI analysis, wildfire research, etc. In addition to this, Landsat 8 data is also instrumental in agriculture, particularly for monitoring crop health and stress levels. Thermal imagery helps detect variations in plant temperature, indicating water stress, nutrient deficiencies, or pest infestations. Farmers and agricultural specialists can leverage this data for optimized irrigation planning, pest management, and yield prediction., wildfire analysis, and detection. While both Band 10 and Band 11 are suitable for thermal studies, the USGS has advised against utilizing TIRS Band 11 due to its higher calibration uncertainty [41-42]. As a result, only Band 10 was employed in this study within this context. Simplified flowchart of the study and applied methods is given in Figure 2.

2.3.1 Top of atmospheric (TOA) spectral radiance

The first step in calculation of the Land Surface Temperature (LST) is TOA spectral radiance calculation. TOA represents a dimensionless value indicating the ratio of reflected radiance to the incident solar radiance reaching the Earth's surface. Its calculation relies on spectral radiance measurements, incorporating the average solar irradiance spectrum and the solar zenith angle. Equation 1 was used to calculate the TOA by using Raster Calculator tool in ArcGIS

Pro. Acquired TOA spectral radiance values are used in the calculation of brightness temperature.

$$L\lambda = ML\ x\ Q_{cal} + AL - O_i \quad (1)$$

M_L: Band-specific multiplicative rescaling factor, Qcal: Pixel values of Band 10, AL: Band-specific additive rescaling factor, Q_i:Band 10 correction value

2.3.2 Conversion of TOA to brightness temperature

Following the acquisition of TOA spectral radiance, the next step is to convert it to brightness temperature. This involves using Planck's Law, which describes spectral radiance as a function of wavelength and temperature, to convert the radiance to brightness temperature [43]. Brightness temperature represents the temperature of a black body emitting the same amount of radiation. For practical use, Planck's Law is often simplified with precomputed sensor-specific constants K1 and K2. Equation 2 used to conversion of TOA spectral radiance to brightness temperature. To obtain the results in Celsius, the radiant temperature is adjusted by subtracting the absolute zero (-273.15°C). Using the same approach applied for the calculation in Equation 1, the Raster Calculator tool in ArcGIS Pro toolbox is employed for Equation 2. In order to use brightness temperature values for the determination of LST, they should be corrected for spectral emissivity (ε). The emissivity correction is based on the type of land cover and is performed using the Normalized Difference Vegetation Index (NDVI), which is calculated in the next step.

$$BT = \left(K2/(ln(K1/L) + 1)\right) - 273.15 \quad (2)$$

K2: Band-specific thermal conversion constant, K1: Band-specific thermal conversion constant from metadata, L: Spectral radiance of TOA

2.3.3 Calculation of normalized difference vegetation index (NVDI)

The Normalized Difference Vegetation Index (NDVI) is a parameter used to calculate LST for brightness temperature correction for spectral emissivity. LST can be used in environmental and agricultural studies and reflects the temperature of the Earth's surface, which can be measured both remotely and on-site. NDVI also provides information about variations in vegetation cover and health, and can be used by researchers to assess the influence of vegetation on thermal measurements [44-46]. NDVI values are calculated using the Raster Calculator tool in ArcGIS Pro toolbox by using Equation 3 for processing. NDVI values also calculate the vegetation cover proportion (Pv).

$$\text{NVDI}=(\text{Band 5}-\text{Band 4})\ /(\text{Band 5}+\text{Band4}) \quad (3)$$

Band 5: Pixel values of Band 5, Band 4: Pixel values of Band 4

2.3.4 Calculation of proportion of vegetation (Pv) and emissivity (ε)

The proportion of vegetation (P_v) is determined using indices like NDVI to calculate the fraction of an area covered by vegetation based on differences between NDVI values and predefined threshold limits for soil and vegetation [47]. Emissivity (ε) measures how efficiently a surface emits thermal radiation depending on surface type and conditions. Emissivity correction in remote sensing is important for accurate temperature measurements for LST to ensure adjustments for vegetation and surface properties for environmental monitoring, agriculture, and climate studies [48]. Equations 4 and 5 calculate the proportion of vegetation and emissivity parameters using the same methodology applied in earlier steps.

$$P_v = (NDVI - NDVI_{min}) - (NVDI_{max} - NDVI_{min}) \quad (4)$$

$$\varepsilon = 0.004 * P_v + 0.986 \quad (5)$$

NVDI: Calculated vegetation index, $NVDI_{min}$: Lowest NDVI value observed, $NVDI_{max}$: Highest NDVI value observed, P_v: Percentage of fraction of an area covered by vegetation, ε: Value of a surface emits thermal radiation

2.3.5 Calculation of land surface temperature (LST)

Applying the previously discussed parameters, Equation 6 calculates pixel-wise Land Surface Temperature (LST) values across the study area. This process involves converting thermal data into radiance, computing brightness temperatures adjusted for emissivity, and finally mapping LST, providing spatial insights into surface temperature variations crucial for environmental monitoring and resource management [49-51].

$$LST = (BT/(1 + (0{,}00115 * BT/1{,}4388) * Ln(\varepsilon))) \quad (6)$$

BT: Brightness temperature, ε: Emissivity value

2.3.6 Urban heat island (UHI)

The conversion of LST values to UHI metrics involves several steps. Initially, LST data, mostly gathered from satellites like Landsat 8, is processed to put forward information about temperature variations over different urban and rural areas. Equation 7 is applied to standardize temperature differences, allowing for the quantification of UHI intensity across the study area.

$$UHI = (LST - LST_{mean})/\ SD \quad (7)$$

LST: Land surface temperature (°C), LST_{mean}: The mean land surface temperature (°C), SD: Standard deviation of temperature

3 Results

This study is considered to offer significant insights into the Urban Heat Island (UHI) phenomenon in the studied area by utilizing Landsat-8. The analysis focused on getting the spatial variations in LST to understand the extent and intensity of UHI within the Kütahya central district and surroundings. A high-resolution UHI map was prepared for the study area using Landsat-8 data to identify the temperature distribution and hotspots with higher

temperature values to characterize the UHI of the Kütahya central district. Another study goal is to provide information for urban planning and sustainable development strategies and approaches. Figure 3 displays the UHI intensity within Kütahya's central area, with hotspots having varying temperatures. Using Landsat 8 data, a UHI map was generated, showing the areas with higher temperatures and corresponding urban areas with minimal vegetation cover. Information about hotspots and insight into the parameters contributing to UHI in the Kütahya central district is also important for urban planning and sustainable development strategies. Figure 3 explains the variation in UHI intensity across the Kütahya central district. These hotspots were classified based on their temperature variations, land use and land cover: urban industrial areas, green zones, rock outcrops, forests, and dense or sparse urbanization. This classification defines how different types of land use and urban morphology contribute to variations in local temperature patterns. Also it provides information about areas with significant UHI effects and cooler spots within the city. The maximum UHI value recorded in the study area was 4.2°C, observed mostly around the rock outcrops (Class 3) located in the northern part of the Kütahya central district, urban industrial site (Class 1) and dense urbanization (Class 5). In contrast, the minimum UHI intensity recorded was -3.5°C along forests (Class 4), sparse urbanization (Class 6) and green spaces (Class 2).

4 Discussions and conclusions

It is believed that this study provides valuable insights in terms of UHI for the study area by using Landsat-8. The analysis of LST variations revealed significant spatial heterogeneity in UHI across the Kütahya urban landscape and surrounding rural regions. High-resolution temperature map derived Landsat-8 data highlighted areas with high-temperature values, mostly observed in dense urban development and rock outcrops, with limited/no vegetation cover. These findings show the impact of urban morphology and land use patterns on local temperature patterns, similar to the previous research highlighting the role of surfaces and reduced green spaces [52-54]. The classification of specific spots within Kütahya based on temperature characteristics further explains the influence of different land cover types on UHI. Areas categorized as urban industrial sites and densely urbanized zones show the highest UHI, reaching up to 4.245°C from average LST values in the study area. These locations typically experience increased heat retention due to the large number of buildings and infrastructure. In contrast, cooler spots within the city, such as forests, sparse urbanized areas, and green spaces, show lower UHI, reaching as low as -3.457°C from average LST values.

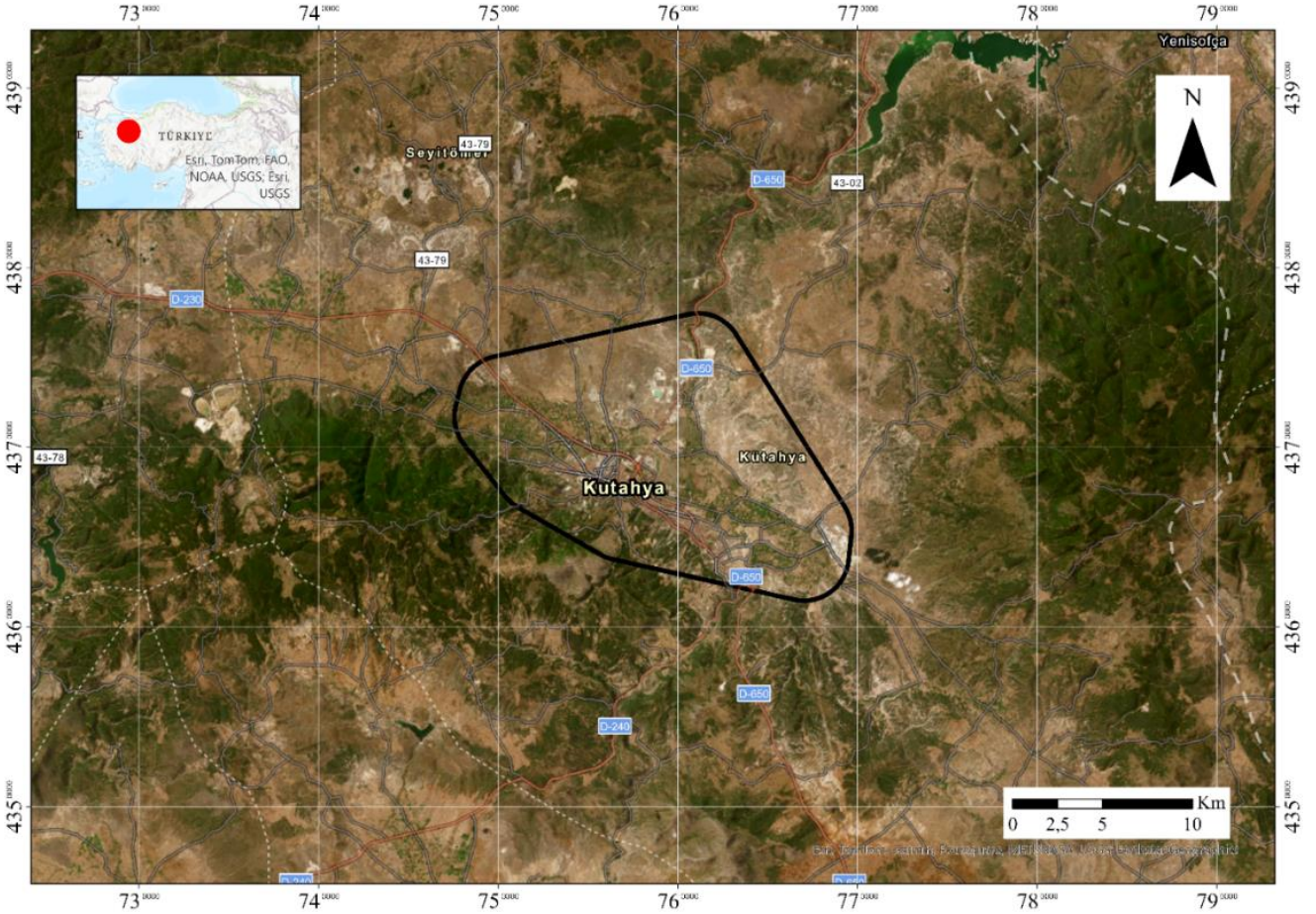

Figure 1. Kütahya central district and general view of the study area.

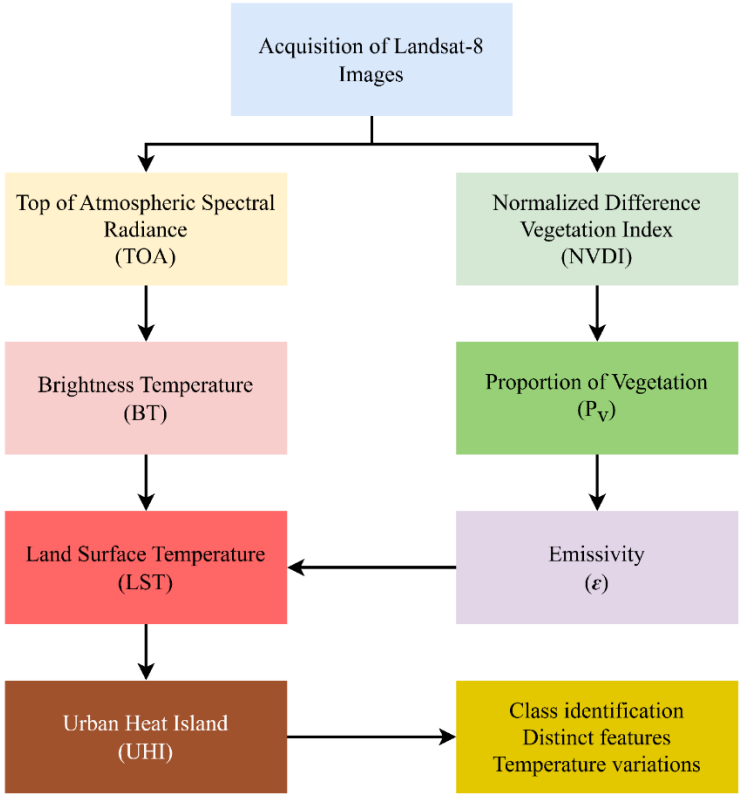

Figure 2. Simplified flow chart of applied methodology.

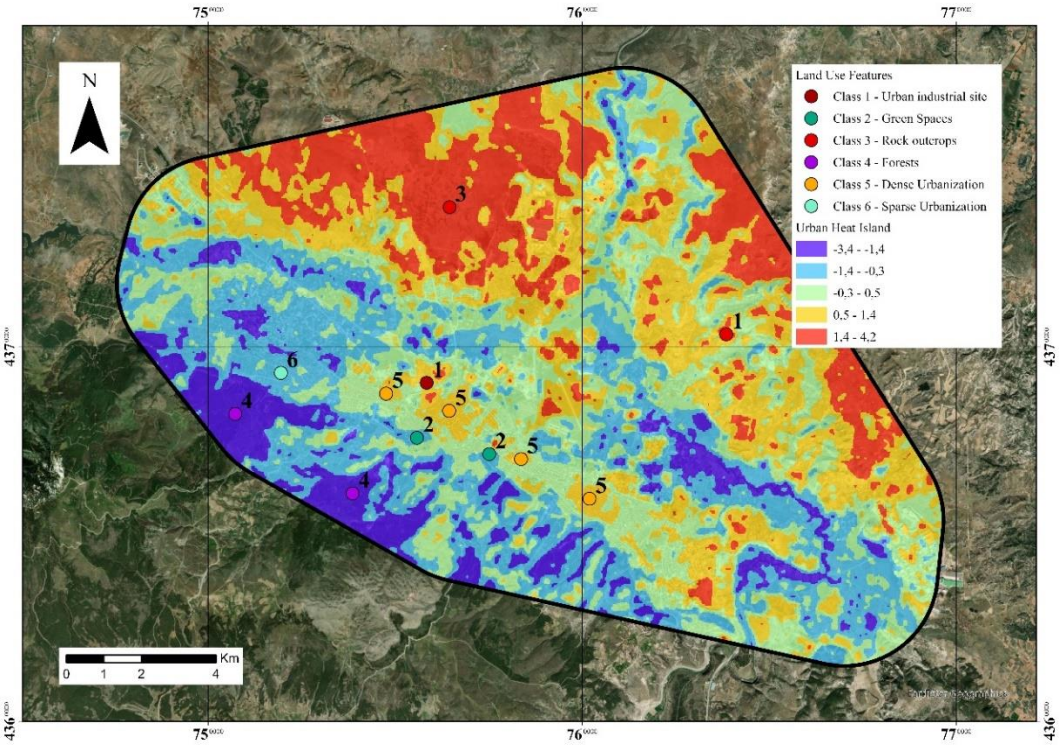

Figure 3. Urban heat island (UHI) and significant land use feature in the study area.

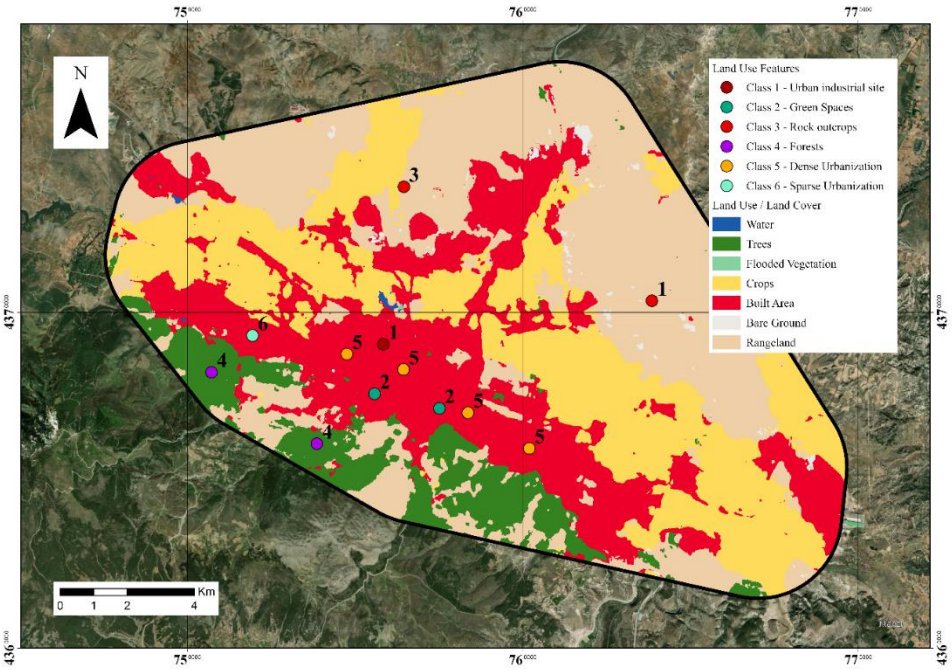

Figure 4. Land Use and Land Cover map of the study area (Simplified from ArcGIS Living Atlas)

In Table 1, zonal statistics comparing land use categories with urban heat island (UHI) data reveal distinct patterns in temperature effects are given. Water and tree-covered areas exhibit a cooling effect with mean UHI values of -1.5°C and -1.7°C, respectively, indicating that these land uses generally mitigate the UHI effect. Flooded vegetation also shows a cooling tendency, with a mean UHI of -1.4°C. In contrast, cropland has a neutral effect on UHI with a mean value of 0.0°C, suggesting it neither significantly warms nor cools the area. Built-up areas and bare ground, on the other hand, contribute to a warming effect, with mean UHI values of 0.2°C and 0.5°C, respectively. Rangeland exhibits the highest mean UHI of 0.8°C, indicating the most pronounced warming effect among the land use categories. The range of UHI values is widest for rangeland (7.3°C) and built-up areas (6.8°C), reflecting considerable variability in temperature effects, while cropland shows a moderate range of 6.1°C. A positive relationship between areas with high temperature differences in terms of UHI effects and land use types is evident in Figures 3 and 4. These figures illustrate that areas experiencing significant temperature variability are closely associated with specific land use categories. For instance, land uses with a pronounced warming effect, such as dense and spare built-up areas and rangeland, show a direct correlation with higher temperature variations. Conversely, land uses that generally cool the environment, like water bodies and tree cover, are associated with lower temperature differences. This correlation underscores the influence of different land uses on the magnitude of UHI effects, providing a clearer understanding of how varying land uses contribute to temperature fluctuations within urban and peri-urban areas.

These findings highlight the cooling effect of vegetation and open spaces in mitigating UHI impacts by providing shade and promoting evaporative cooling processes.

Table 1. Zonal statistics comparing land use and urban heat island data.

Class Name	Min	Max	Range	Mean	STD
Water	-2.4	-0.1	2.3	-1.5	0.5
Trees	-3.5	0.9	4.4	-1.7	0.8
Flooded Vegetation	-1.8	1.0	2.8	-1.4	0.7
Crops	-2.7	3.4	6.1	0.0	1.1
Built Area	-3.1	3.6	6.8	0.2	0.8
Bare Ground	-1.2	2.4	3.6	0.5	0.8
Rangeland	-3.1	4.2	7.3	0.8	1.0

In conclusion, this study spotlights the spatial variability of UHI intensity in Kütahya's central district. It underscores the importance of considering urban planning strategies integrating green infrastructure and sustainable development practices. The use of Landsat-8 satellite data proved instrumental in mapping and understanding UHI dynamics, providing a comprehensive spatial analysis of temperature variations across different land use categories. Addressing UHI challenges requires proactive measures such as increasing urban greenery, promoting cool roof technologies, changing asphalt colour, environmentally building paints and implementing heat-resilient urban design principles. These efforts are very important for improving urban life quality, reducing energy consumption, and mitigating the adverse effects of climate change in urban areas like Kütahya. New technologies like UAV mapping, field-based measurements can also create more detailed

UHI, enabling extensive and detailed evaluations for urban cooling strategies, surface heat monitoring, capturing small-scale surface temperature variations, etc. [55-57] Implementing high-resolution Land Surface Temperature (LST) mapping using UAVs and on-site measurements can create more accurate and localized maps. These maps would benefit local authorities and researchers, providing valuable insights for urban planning.

Acknowledgements

The authors gratefully acknowledge Kütahya Dumlupınar University for granting access to ArcGIS Pro software.

Declatation of Competing Interest

The authors declare that they have no known competing financial interests or personal relationships that could have appeared to influence the work reported in this paper.

Similarty rate (iThenticate): 16%

References

[1] M.K. Anser, M. Alharthi, B. Aziz, S. Wasim, Impact of urbanization, economic growth, and population size on residential carbon emissions in the SAARC countries, Clean Technologies and Environmental Policy. 22, 923-936, 2022. doi:10.1007/s10098-020-01833-y.

[2] L. Howard, The Climate of London, Harvey and Dorton. I-II (1883).

[3] K. Kłysik, K. Fortuniak, Temporal and spatial characteristics of the urban heat island of Łódź, Poland, Atmospheric Environment. 33 3885-3895, 1999. doi:10.1016/S1352-2310(99)00131-4.

[4] H. Li, Y. Zhou, G. Jia, K. Zhao, J. Dong, Quantifying the response of surface urban heat island to urbanization using the annual temperature cycle model, Geoscience Frontiers. 13 101141, 2022. doi:10.1016/j.gsf.2021.101141.

[5] L. Li, Y. Zha, R. Wang, Relationship of surface urban heat island with air temperature and precipitation in global large cities, Ecological Indicators. 117, 106683, 2020. doi:10.1016/j.ecolind.2020.106683.

[6] S. Barrao, R. Serrano-Notivoli, J.M. Cuadrat, E. Tejedor, M.A. Saz Sánchez, Characterization of the UHI in Zaragoza (Spain) using a quality-controlled hourly sensor-based urban climate network, Urban Climate.44 101207, 2022. doi:10.1016/j.uclim.2022.101207.

[7] X. Gui, L. Wang, R. Yao, D. Yu, C. Li, Investigating the urbanization process and its impact on vegetation change and urban heat island in Wuhan, China, Environmental Science and Pollution Research. 26, 30808-30825, 2019. doi:10.1007/s11356-019-06273-w.

[8] H. Takebayashi, M. Moriyama, Relationships between the properties of an urban street canyon and its radiant environment: Introduction of appropriate urban heat island mitigation technologies, Solar Energy. 86, 2255-2262, 2012. doi:10.1016/j.solener.2012.04.019.

[9] G. Ferguson, A.D. Woodbury, Urban heat island in the subsurface, Geophysical Research Letters. 34, GL032324, 2007. doi:10.1029/2007GL032324.

[10] K. Menberg, P. Blum, A. Schaffitel, P. Bayer, Long-Term Evolution of Anthropogenic Heat Fluxes into a Subsurface Urban Heat Island, Environmental Science & Technology. 47, 9747-9755, 2013. doi:10.1021/es401546u.

[11] H.N. Pollack, S. Huang, P.-Y. Shen, Climate Change Record in Subsurface Temperatures: A Global Perspective, Science. 282, 279-281, 1998. doi:10.1126/science.282.5387.279.

[12] K.P. Gallo, T.W. Owen, Satellite-Based Adjustments for the Urban Heat Island Temperature Bias, Journal of Applied Meteorology. 38, 806-813, 1999. doi:10.1175/1520-0450(1999)038<0806:SBAFTU>2.0.CO;2.

[13] F. Perrier, J.-L. Le Mouël, J.-P. Poirier, M.G. Shnirman, Long-term climate change and surface versus underground temperature measurements in Paris, International Journal of Climatology. 25, 1619-1631, 2005. doi:10.1002/joc.1211.

[14] R.A. Spronken-Smith, T.R. Oke, Scale Modelling of Nocturnal Cooling in Urban Parks, Boundary-Layer Meteorology. 93, 287-312, 1999. doi:10.1023/A:1002001408973.

[15] M. Taniguchi, T. Uemura, K. Jago-on, Combined Effects of Urbanization and Global Warming on Subsurface Temperature in Four Asian Cities, Vadose Zone Journal. 6 591-596, 2007. doi:10.2136/vzj2006.0094.

[16] K. Kataoka, F. Matsumoto, T. Ichinose, M. Taniguchi, Urban warming trends in several large Asian cities over the last 100 years, Science of The Total Environment. 407, 3112-3119, 2009. doi:10.1016/j.scitotenv.2008.09.015.

[17] M. Karaca, Ü. Anteplioğlu, H. Karsan, Detection of urban heat island in Istanbul, Turkey, Il Nuovo Cimento C. 18 (1), 995, 49-55. doi:10.1007/BF02561458.

[18] Y. Ezber, O. Lutfi Sen, T. Kindap, M. Karaca, Climatic effects of urbanization in istanbul: a statistical and modeling analysis, International Journal of Climatology. 27, 667-679, 2007. doi:10.1002/joc.1420.

[19] O.S. Pinho, M.D.M. Orgaz, The urban heat island in a small city in coastal Portugal, International Journal of Biometeorology. 44, 198-203, 2020. doi:10.1007/s004840000063

[20] A.S. Öngen, Z.A. Ergüler, The effect of urban heat island on groundwater located in shallow aquifers of Kutahya city center and shallow geothermal energy potential of the region, Bulletin Of The Mineral Research and Exploration. 1-24, 2020. doi:10.19111/bulletinofmre.820395.

[21] R.U. Acar, C. Özkul, Investigation of heavy metal pollution in roadside soils and road dusts along the Kütahya–Eskişehir Highway, Arabian Journal of Geosciences. 13, 216, 2020. doi:10.1007/s12517-020-5206-2.

[22] R.U. Acar, E. Zengin, Performance Assessment of Landsat 8 and Sentinel-2 Satellite Images for the Production of Time Series Land Use/Land Cover (LULC) Maps, Journal of Scientific Reports-A. 1-15, 2023. doi:10.59313/jsr-a.1213548.

[23] M. Bagyaraj, V. Senapathi, S. Karthikeyan, S.Y. Chung, R. Khatibi, A.A. Nadiri, B. Asgari Lajayer, A study of urban heat island effects using remote sensing and GIS techniques in Kancheepuram, Tamil Nadu, India, Urban Climate. 51, 101597, 2023. doi:10.1016/j.uclim.2023.101597.

[24] B. Doğan, F. Şen, E. Zengin, S. Alaçam, N. Çakıcı Alp, Tectonic Model of the Surface Ruptures Geometry of M 7.7 and M 7.6 Earthquakes, of Their Source Faults of Kahramanmaraş (Türkiye) on 06/02/2023, içinde: Chamber of Geological Engineers of Türkiye, Ankara, Türkiye, 2023.

[25] R. Eker, A. Aydın, J. Hübl, Unmanned aerial vehicle (UAV)-based monitoring of a landslide: Gallenzerkogel landslide (Ybbs-Lower Austria) case study, Environmental Monitoring and Assessment. 190, 28, 2017. doi:10.1007/s10661-017-6402-8.

[26] Z.A. Erguler, E. Zengin, G. Kalyoncu Erguler, Time-dependent physicomechanical behavior of ballasts used for railway between Sabuncupinar and Kütahya in Western Turkey, Environmental Earth Sciences. 75 918, 2016. doi:10.1007/s12665-016-5724-0.

[27] K.M. Nissen, M. Wilde, T.M. Kreuzer, A. Wohlers, B. Damm, U. Ulbrich, A decrease in rockfall probability under climate change conditions in Germany, Natural Hazards and Earth System Sciences. 23, 2737-2748, 2023. doi:10.5194/nhess-23-2737-2023.

[28] E. Zengin, Inundation risk assessment of Eastern Mediterranean Coastal archaeological and historical sites of Türkiye and Greece, Environmental Monitoring and Assessment. 195, 968, 2023. doi:10.10 07/s10661-023-11549-3.

[29] E. Zengin, A Combined Assessment of Sea Level Rise (SLR) Effect on Antalya Gulf (Türkiye) and Future Predictions on Land Loss, Journal of the Indian Society of Remote Sensing. 51, 1121-1133, 2023. doi:10.1007/s12524-023-01694-0.

[30] E. Zengin, Z.A. Erguler, Experimental investigation of pore-fracture relationship on failure behaviour of porous rock materials, Bulletin of Engineering Geology and the Environment. 81, 351, 2022. doi:10.1007/s10064-022-02857-y.

[31] C. Keeratikasikorn, S. Bonafoni, Urban Heat Island Analysis over the Land Use Zoning Plan of Bangkok by Means of Landsat 8 Imagery, Remote Sensing. 10, 440, 2018. doi:10.3390/rs10030440.

[32] V.I. Kashtan, K.L. Serhieieva, O.V. Korobko, D.V. Ivanov, Search and assessment of urban heat islands on digital satellite images, System Technologies. 3, 87-98, 2023. doi:10.34185/1562-9945-3-146-2023-09.

[33] G. Seeberg, A. Hostlowsky, J. Huber, J. Kamm, L. Lincke, C. Schwingshackl, Evaluating the Potential of Landsat Satellite Data to Monitor the Effectiveness of Measures to Mitigate Urban Heat Islands: A Case Study for Stuttgart (Germany), Urban Science. 6, 82, 2022. doi:10.3390/urbansci6040082.

[34] N. Aslan, D. Koc-San, The Use of Land Cover Indices for Rapid Surface Urban Heat Island Detection from Multi-Temporal Landsat Imageries, ISPRS International Journal of Geo-Information. 10, 416, 2021. doi:10.3390/ijgi10060416.

[35] C.R.D. Almeida, L. Furst, A. Gonçalves, A.C. Teodoro, Remote Sensing Image-Based Analysis of the Urban Heat Island Effect in Bragança, Portugal, Environments. 9, 98, 2022. doi:10.3390/environments9080098.

[36] N. Na, D. Xu, W. Fang, Y. Pu, Y. Liu, H. Wang, Automatic Detection and Dynamic Analysis of Urban Heat Islands Based on Landsat Images, Remote Sensing. 15, 4006, 2023. doi:10.3390/rs15164006.

[37] M. Kottek, J. Grieser, C. Beck, B. Rudolf, F. Rubel, World Map of the Köppen-Geiger Climate Classification Updated, Meteorologische Zeitschrift. 15, 259-263, 2006. doi:10.1127/0941-2948/2006/0130.

[38] M.C. Anderson, J.M. Norman, W.P. Kustas, R. Houborg, P.J. Starks, N. Agam, A thermal-based remote sensing technique for routine mapping of land-surface carbon, water and energy fluxes from field to regional scales, Remote Sensing of Environment. 112, 4227-4241, 2008. doi:10.1016/j.rse.2008.07.009.

[39] N.A. Brunsell, R.R. Gillies, Length Scale Analysis of Surface Energy Fluxes Derived from Remote Sensing, Journal of Hydrometeorology. 4, 1212-1219, 2003. doi:10.1175/1525-7541(2003)004<1212:LSAOSE>2.0.CO;2.

[40] A. Karnieli, N. Agam, R.T. Pinker, M. Anderson, M.L. Imhoff, G.G. Gutman, N. Panov, A. Goldberg, Use of NDVI and Land Surface Temperature for Drought Assessment: Merits and Limitations, Journal of Climate. 23, 618-633, 2010. doi:10.1175/2009JCLI2900.1.

[41] U. Avdan, G. Jovanovska, Algorithm for Automated Mapping of Land Surface Temperature Using LANDSAT 8 Satellite Data, Journal of Sensors. e1480307, 2016. doi:10.1155/2016/1480307.

[42] J.A. Barsi, J.R. Schott, S.J. Hook, N.G. Raqueno, B.L. Markham, R.G. Radocinski, Landsat-8 Thermal Infrared Sensor (TIRS) Vicarious Radiometric Calibration, Remote Sensing. 6, 11607-11626, 2014. doi:10.3390/rs61111607.

[43] H.D. Young, R.A. Freedman, University Physics with Modern Physics, Pearson Education, 2015.

[44] S. Mohanasundaram, T. Baghel, V. Thakur, P. Udmale, S. Shrestha, Reconstructing NDVI and land surface temperature for cloud cover pixels of Landsat-8 images for assessing vegetation health index in the Northeast region of Thailand, Environmental Monitoring and Assessment. 195, 211, 2022. doi:10. 1007/s10661-022-10802-5.

[45] A. Naga Rajesh, S. Abinaya, G. Purna Durga, T.V. Lakshmi Kumar, Long-term relationships of MODIS NDVI with rainfall, land surface temperature, surface

soil moisture and groundwater storage over monsoon core region of India, Arid Land Research and Management. 37, 51-70, 2023. doi:10.1080/15324982.2022.2106323.

[46] W. Ullah, K. Ahmad, S. Ullah, A.A. Tahir, M.F. Javed, A. Nazir, A.M. Abbasi, M. Aziz, A. Mohamed, Analysis of the relationship among land surface temperature (LST), land use land cover (LULC), and normalized difference vegetation index (NDVI) with topographic elements in the lower Himalayan region, Heliyon. 9, e13322, 2023. doi:10.1016/j.heliyon.2023.e13322.

[47] S. Ma, L.-J. Wang, L. Ye, J. Jiang, Vegetation restoration thresholds under different vegetation types and altitude gradients in the Sichuan-Yunnan ecological shelter, China, Journal of Environmental Management. 340, 117910, 2023. doi:10.1016/j.jenvman.2023.117910.

[48] C. Ru, S.-B. Duan, X.-G. Jiang, Z.-L. Li, C. Huang, M. Liu, An extended SW-TES algorithm for land surface temperature and emissivity retrieval from ECOSTRESS thermal infrared data over urban areas, Remote Sensing of Environment. 290, 113544, 2023. doi:10.1016/j.rse.2023.113544.

[49] Y. Chen, J. Yang, W. Yu, J. Ren, X. Xiao, J.C. Xia, Relationship between urban spatial form and seasonal land surface temperature under different grid scales, Sustainable Cities and Society. 89, 104374, 2023. doi:10.1016/j.scs.2022.104374.

[50] A. Tariq, F. Mumtaz, M. Majeed, X. Zeng, Spatio-temporal assessment of land use land cover based on trajectories and cellular automata Markov modelling and its impact on land surface temperature of Lahore district Pakistan, Environmental Monitoring and Assessment. 195, 114, 2022. doi:10.1007/s10661-022-10738-w.

[51] M. Zhang, A.-A. Kafy, P. Xiao, S. Han, S. Zou, M. Saha, C. Zhang, S. Tan, Impact of urban expansion on land surface temperature and carbon emissions using machine learning algorithms in Wuhan, China, Urban Climate. 47, 101347, 2023. doi:10.1016/j.uclim.2022.101347.

[52] C. Wang, Z. Ren, Y. Dong, P. Zhang, Y. Guo, W. Wang, G. Bao, Efficient cooling of cities at global scale using urban green space to mitigate urban heat island effects in different climatic regions, Urban Forestry & Urban Greening. 74, 127635, 2022. doi:10.1016/j.ufug.2022.127635.

[53] X.D. Xiao, L. Dong, H. Yan, N. Yang, Y. Xiong, The influence of the spatial characteristics of urban green space on the urban heat island effect in Suzhou Industrial Park, Sustainable Cities and Society. 40, 428-439, 2018. doi:10.1016/j.scs.2018.04.002.

[54] W. Zhou, W. Yu, Z. Zhang, W. Cao, T. Wu, How can urban green spaces be planned to mitigate urban heat island effect under different climatic backgrounds? A threshold-based perspective, Science of The Total Environment. 890, 164422, 2023. doi:10.1016/j.scitotenv.2023.164422.

[55] J. Ahmad, J.A. Eisma, Capturing Small-Scale Surface Temperature Variation across Diverse Urban Land Uses with a Small Unmanned Aerial Vehicle, Remote Sensing. 15, 2042, 2023. doi:10.3390/rs15082042.

[56] Y.-I. Cho, D. Yoon, M.-J. Lee, Comparative Analysis of Urban Heat Island Cooling Strategies According to Spatial and Temporal Conditions Using Unmanned Aerial Vehicles(UAV) Observation, Applied Sciences. 13, 10052, 2023. doi:10.3390/app131810052.

[57] K.A. Henn, A. Peduzzi, Surface Heat Monitoring with High-Resolution UAV Thermal Imaging: Assessing Accuracy and Applications in Urban Environments, Remote Sensing. 16, 930, 2024. doi:10.3390/rs16050930.